American Journal of Environmental Engineering and Science
2014; 1(1): 19-35
Published online September 30, 2014 (http://www.aascit.org/journal/ajees)

American Association for Science and Technology

A remote sensing technique detecting and identifying water activity sites along irrigation canals

Muhammad Arshad[1, *], Richard Gomez[2], Allan Falconer[2], William Roper[2], Michael Summers[3]

[1]Department of Chemical Engineering, King Khalid University, Abha, Kingdom of Saudi Arabia
[2]Department of Geography and Geoinformation Sciences, George Mason University, Fairfax, USA
[3]Department of Physics and Astronomy, George Mason University, Fairfax, USA

Email address

Marshad205@gmail.com (M. Arshad)

Keywords

Airborne Sensors,
Near-Infrared,
Thermal-Infrared,
Google Earth,
Multispectral,
Irrigation Canals,
Seepage,
Water-logging

Received: August 25, 2014
Revised: September 04, 2014
Accepted: September 05, 2014

Citation

Muhammad Arshad, Richard Gomez, Allan Falconer, William Roper, Michael Summers. A Remote Sensing Technique Detecting and Identifying Water Activity Sites Along Irrigation Canals. *American Journal of Environmental Engineering and Science*. Vol. 1, No. 1, 2014, pp. 19-35.

Abstract

One of the consequences of climatic change is that many western states in the United States are experiencing severe drought conditions. Numerous irrigation districts are losing significant amounts of water from their canal systems due to leakage. Every year, on the average 2 million acres of prime cropland in the US is lost to soil erosion, waterlogging and salinity. Lining of canals could save enormous amount of water for irrigating crops but due to soaring costs of construction and environmental mitigation, adopting such programs on a large scale would be excessively expensive. Conventional techniques of seepage detection are expensive, time consuming and labor intensive, and in addition are generally not very accurate. Technological advancements have made it possible to investigate irrigation canals for seepage site identification using remote sensing. In this research, band-9 in the NIR region and band-45 in the TIR region of airborne MASTER data has been utilized to highlight anomalies along irrigation canals in Phoenix, Arizona. A high resolution (1 to 4 meter pixels) satellite image provided by private companies, which has been made available to the public by the Google Earth, was then successfully used to separate those anomalies into water activity sites, natural vegetation, and man-made structures. We show that regions for which such high resolution satellite images are available on Google Earth can be successfully utilized for verification of anomalies along irrigation canals using airborne multispectral data. This innovative technique is much faster and cost effective compared to conventional and past airborne remote sensing techniques for verification of anomalies along irrigation canals. This technique also solves the long standing problem of discriminating true water related activities from false impressions of seepage sites due to dense natural vegetation, terrain relief and low depressions of natural drainages.

1. Introduction

Irrigated agriculture is estimated to be practiced on 270 million ha around the world, comprising 17% of the total arable land, and producing almost one third of the total food production. India, China, United States, and Pakistan posses more than half of the world's irrigated land (Ahmad, 2002). Numerous irrigation districts in many of the western states of the US are losing a significant amount of water from their canal systems due to leakage. Every year on the average 2 million acres of prime cropland in the US is lost to soil erosion, waterlogging and salinity (Pimentel and Giampietro, 1994).

Canals systems are usually unlined and as a consequence loose water due to seepage. This results not only in reduced water for crops but also in waterlogging near the canals (Snell, 2001). Swan (1978) and many others are of the view that much of the irrigated land in the world is losing productivity, or being abandoned, because of the inability to control groundwater below the irrigated land. According to the United Nations Economic and Social Commission for Asia (UN-ESCAP) estimates of water-logging and salinity affected areas have exceeded 1 million ha in Cambodia and Thailand, 3 million ha in Afghanistan, Bangladesh, Mongolia and Malaysia, 10 million ha in Pakistan and Indonesia, 20 million ha in China, India and Iran and 350 million ha in Australia (Szabolcs 1979 as cited in Asif and Ahmad, 2002). Recent research statistics show that arable land loss relating to salt affected areas are close to 1 billion hectares, which represents about 7% of the Earth's continental surface area (Ghassemi et al., 1995, cited in Metternicht, 2003).

According to Swan (1978) an unlined canal excavated in clay would be fairly water tight. But in clayey loam a typical canal will lose about 150 l $d^{-1}m^{-2}$ of wetted area, 250 l $d^{-1}m^{-2}$ in sandy loam, and 750 l $d^{-1}m^{-2}$ or more in gravel soil. In non saline areas, the water lost through seepage is sometimes beneficial as it recharges the underground aquifers. (Sakthivadivel et al. 2001; King and Sheng, 2002; Wachyan and Rushton, 1987).

Seepage detection is especially important at places where the canal is elevated above the surrounding terrain on one or both sides. These embankments should be regularly inspected for leakages; otherwise, if leaks develop it could lead to complete collapse of embankments (Washburn, 2002). Water use efficiency in developing countries are typically 30-50%, and in some, only 20-30%; yet few effective water conservation programs exist and most countries do not monitor irrigation system performance and management (Walker, 1999; Hennessy, 1993). The cost of water that can be saved through canal improvements is about 25 percent of the cost of developing an equal volume of new water supply (World Bank Report, 1995 cited in Sakathivadivel, 2001). However, investment in conducting such projects has slowed due to soaring construction costs.

Water supplies for irrigation can be increased by lining the canals. Lining has many advantages such as reduction in seepage losses, increase in discharge capacity for a given section, stabilization of the banks, protection of the canal bed and banks from erosion, and reduction in maintenance costs (Gawad et al., 1993, Snell 2001). Thus lining of irrigation canals could save substantial amounts of water, but the costs of adopting such programs are excessive. Un-reinforced concrete lining is the most common and normally reduces the loss of water to less than 15 l $d^{-1}m^{-2}$. Most of the water is lost through joints or cracks (Swan, 1978). According to King and Sheng (2002), lining an irrigation ditch that is 30 inches deep with one-foot-wide bottom could cost $100,000 a mile. Lining larger canals can cost from $600,000 to $1 million a mile for lining. However, at the same time very small imperfections in the canal linings will render it useless (Gawad et al., 1993). The cost estimates on lining types range from $5 - $40 per square meter for existing canals (Snell, 2001).

2. Conventional and Geospatial Techniques for Leak Detection

Some of the most common techniques used for seepage detection in the literature are the inflow outflow method, the pondage test method and the seepage meter method. Generally, pondage tests are regarded as the most accurate method of seepage estimation, although most authors note that every method has certain disadvantages (Critchley and Aikman, 1994 cited in Pickerill and Malthus, 1998). However, the amount of time utilized in locating a seepage area and the associated rising costs of labor and transportation is straining the limiting financial resources of countries. The high costs severely limits extensive efforts of mapping seepage sites along irrigation canals with existing conventional techniques especially in large irrigation districts. These conventional techniques also often do not precisely locate leaks. There is an urgent need for alternative techniques that are fast, accurate, cost effective and which can be successfully utilized without altering the smooth operation of canal water distribution for irrigation of crops.

Many researchers have attempted to utilize remote sensing for seepage detection along canals but were only partially successful due to the difficulty of separating dry areas in shadows such as tree shades, low depression areas of natural drainage, and paved roads from wet areas (Nellis, 1982; Pickerill and Malthus, 1998). Most of the earlier researchers processed their image data for seepage sites detection and the anomalies found on the imagery were inferred as possible leakage sites. The images with anomalies were then overlaid with either U.S. Geological Survey topographic maps or Digital Ortho-photo Quarter Quadrangles (DOQQs). Once the locations were determined, field checks, which involve substantial time and travelling costs, were made to verify the detected anomalies.

The strategy discussed in the following pages is to make use of the high resolution (1 to 4 meter per pixel) satellite images that have been made available by private companies to the scientific community for research purposes. Google has made Earth image archives available to the public on Google Earth. In this study, MODIS/ASTER Airborne Simulator (MASTER) data scenes provided by the airborne sensor facility of National Aeronautics and Space Administration (NASA) Ames research center, Moffett Field, California were calibrated and then processed for geometric and radiometric correction. Scenes were then mosaicked and masked for the delineation of canal segments. A density slicing technique (AbdelSalam et al, 2000; Yamano et al, 2006; Klemas et al, 1973; Whiteman and Brown, 1998) was applied to the gray scale image (masked area in band-9) by carefully considering the ranges of radiance values of pixels for highlighting anomalies along irrigation canals. Anomalies detected on the imagery along irrigation canals were investigated for water activity, shadows of various natures, paved roads, and a variety of other effects. The co-ordinates of the observed anomalies were fed into a search text box at Google Earth and were verified for the anomaly observed on the imagery by zooming to a perspective of few hundred feet above the target area. This procedure reduces the cost and labor of obtaining topographic maps or DOQQs and also reduces the processing time involved such as overlaying images over DOQQs for determining the location of anomaly along irrigation canal.

The other monetary advantage of using this technique is in reduced travel costs. False seepage sites (e.g., tree shadows or terrain relief) can be easily excluded using Google Earth. Travel is needed to visit only potential seepage sites. One of the frequent problems with DOQQs and U.S. geological survey topographic maps is that the maps are roughly 5 to 6 years old and not compatible with the recently obtained imagery. Google Earth on the other hand is frequently updated when better imagery is available.

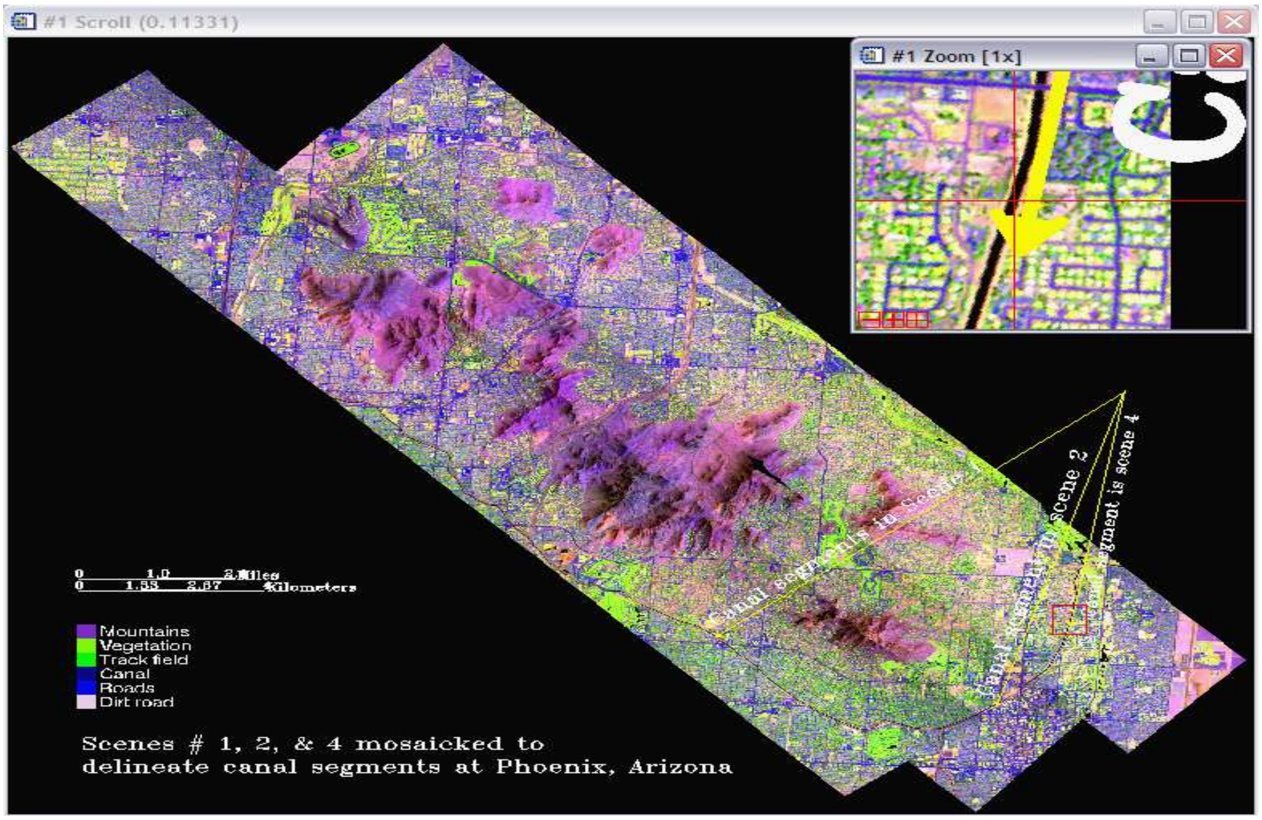

Fig. 3.1. *Spatial subset of scenes 1, 2 and 4 mosaicked to see canal alignment and union of canal segments for analysis*

3. Data Processing

MASTER scenes were calibrated utilizing embedded calibration algorithms provided in the header files of each scene. After scene calibration, the scenes were resized into Digital Elevation Model-Visible-Near-infrared-Shortwave-infrared (DEM-VNIR-SWIR) bands 1 through 25 subset files and Digital Elevation Model-Thermal-infrared (DEM-TIR) bands 41 through 50 subset files. FLAASH software, an ENVI's plug-in module for atmospheric correction, can easily correct hyperspectral and multispectral scenes collected in either vertical or slant viewing geometries. FLAASH software is also capable of retrieving water content per pixel of image (FLAASH software manual). However, FLAASH software requires that the scenes for atmospheric correction should contain bands in the 15 nm spectral resolutions or better. As the channel width of MASTER bands varies between 40 and 650 nm, therefore FLAASH atmospheric correction software could not be performed in a better way.

Table 3.1. *Summary characteristics of MASTER instrument (Source: Modified from X. Chen et al., 2007)*

Characteristics	Band width (μm)
Wavelength range	0.4 – 13 μm
Number of channels	50
Channel width	Varies 40 to 650 nm
Instantaneous field of view	2.5 mrad
Total field of view	85.92°
Number of pixels	716
Platform	B200, ER-2, DC-8
Digitization	16-bit
Number of Spectrometers	4

Severe distortion was observed on inspecting MASTER scenes. Distortion was removed by georeferencing MASTER scenes using embedded pixel latitudes and longitudes from the scene header files. MASTER scenes 1, 2, and 4 were then mosaicked and examined for geo-correction of pixels alignment. It was observed that they were in perfect alignment.

The analysis of MASTER scenes draped on DEM data, as seen in figure 3.1, revealed that most of the scenes are acquired over thickly populated urban areas. Most of the canal segments in the Western Central Salt River (Western CSR) valley are flowing through urban areas and water leakages are rarely expected. Figure 3.2 shows scene # 08 draped over DEM data. It is the only scene which has a segment of canal where some scattered agriculture is seen surrounded by man-made structures.

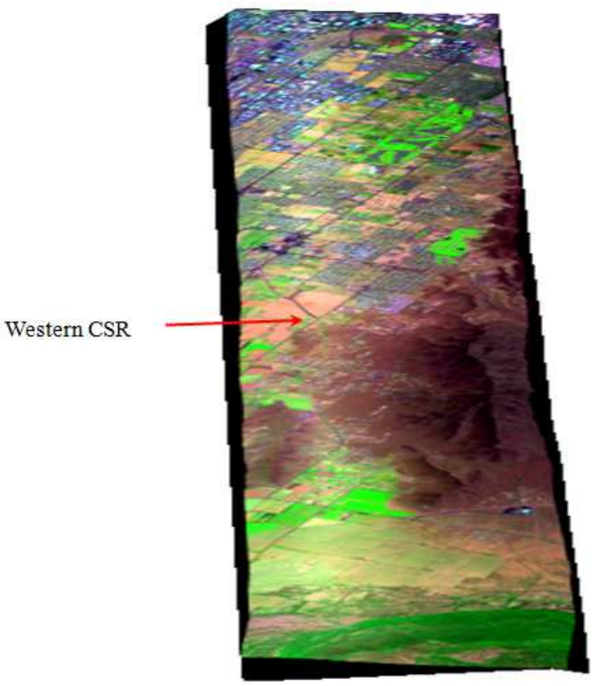

Fig. 3.2. *Scene # 08 overlaid over DEM data showing scattered agriculture along western CSR*

4. Bands Selection

MASTER sensor has 50 bands, with first 25 bands covering VNIR-SWIR regions 15 bands covering MIR region and the last 10 bands cover the TIR region. Table 4.1 excludes MIR region.

Table 4.1. *MODIS/ASTER Airborne Simulator (MASTER) bands (Source: From Kay et al. 2003)*

MASTER Band	Minimum (μm)	Maximum (μm)	Effective Center (μm)
Visible/near-infrared (VNIR)			
1	0.44	0.48	0.46
2	0.48	0.52	0.50
3	0.52	0.56	0.54
4	0.56	0.60	0.58
5	0.63	0.69	0.66
6	0.69	0.74	0.71
7	0.73	0.78	0.75
8	0.78	0.83	0.80
9	0.85	0.89	0.87
10	0.89	0.93	0.91
11	0.93	0.97	0.95
Short-wave infrared (SWIR)			
12	1.59	1.65	1.62
13	1.65	1.70	1.68
14	1.70	1.75	1.73
15	1.75	1.81	1.78
16	1.81	1.86	1.83
17	1.86	1.91	1.88
18	1.91	1.96	1.93
19	1.96	2.01	1.98
20	2.06	2.11	2.08
21	2.14	2.19	2.17
22	2.19	2.24	2.22
23	2.24	2.29	2.26
24	2.30	2.37	2.33
25	2.37	2.42	2.39
Thermal Infrared (TIR)			
41	7.70	8.04	7.86
42	8.07	8.50	8.28
43	8.51	8.90	8.71
44	8.97	9.36	9.18
45	9.64	10.04	9.82
46	10.06	10.47	10.26
47	10.50	11.11	10.80
48	11.18	11.86	11.51
49	12.08	12.59	12.33
50	12.82	13.30	13.06

Frazier and Page (2000) compared the ability of different bands to delineate waterlines in flood plains and muddy tidal flats. But the spatial resolutions of current satellite sensors, which depend on wavelength, limit the accuracy of waterline mapping with current techniques. Yamano et al. (2006) examined various satellite sensor bands for water line extraction at coral reef coasts (Majuro Atoll, Marshall islands) and found a better response for NIR bands as compared to SWIR bands using different spatial resolution (4, 15, and 30 m). Similar studies should be done for detection of water activity locations along irrigation canals using airborne sensors. Low flying aircraft have higher spatial resolution and flexibility of data acquisition for target areas than satellites. Water absorbs efficiently in the near infrared NIR, SWIR and TIR wavelength regions creating a prominent land-water boundary in the image.

It can be observed in Fig. 4.1 that buildings show up as white in the TIR bands (right side) due to the heat radiating from their roofs, while in the NIR image (left side), rooftops of houses tend to appear gray as they do not reflect the sun’s energy strongly in this band.

On the other hand, as can be observed in Fig. 4.2, vegetation such as grass and trees appear brighter in the near-IR band (left side) and gray or darker in TIR bands (right side). The reason is that vegetation strongly reflects solar energy in the NIR bands whereas it absorbs efficiently in TIR bands. Water appears black as it absorbs substantial light in the NIR, SWIR and TIR wavelength regions creating a prominent land-water boundary in the image. The water in the canal (see Fig. 4.2) appears black as the temperature of the water is much cooler than the surrounding land. For prominent land-water boundary delineation of irrigation canals in the MASTER scenes, band 9 from the NIR region is the best candidate, as it eliminates the vegetation which can give a false impression of seepage (appear dark when observed with TIR bands) by giving it brighter tone in the image (see figures 4.3 and 4.4).

The same area when seen in band 45 from the TIR region of MASTER data also gives a false impression of seepage site (see figure 4.4).

This area when viewed for the anomaly (brightness in NIR band 9 and dark patches in TIR band 45) by entering its co-ordinates into Google Earth search text box revealed that these are trees and not seepage sites. Thus Google Earth is a better tool to quickly verify the anomaly found in a thermal band which can then be easily eliminated from the list of suspected seepage sites (see figure 4.5).

Fig. 4.1. *MASTER bands displayed showing contrast between roof tops (Red box). NIR band-9 (0.8690 μm) on left side and TIR band 45 (9.744 μm) on right side*

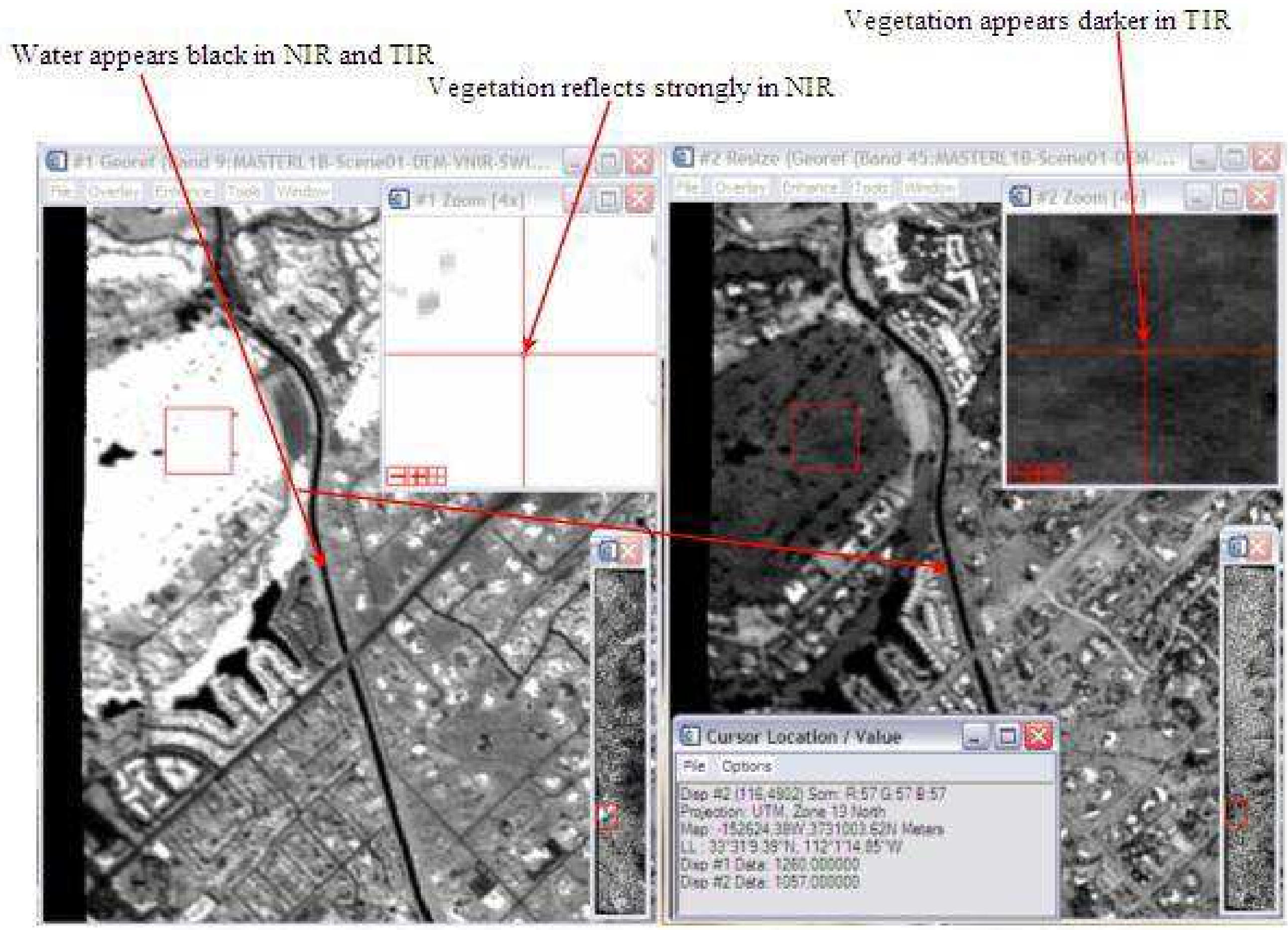

Fig. 4.2. *MASTER bands displayed showing contrast between vegetation (Red box). NIR band-9 (0.8690 μm) on left side and TIR band 45 (9.744 μm) on right side*

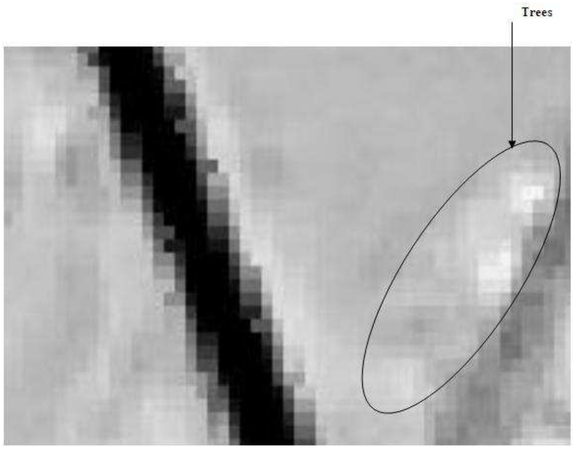

Fig. 4.3. *Trees expression as observed in band 9 from [NIR] region along Western CSR*

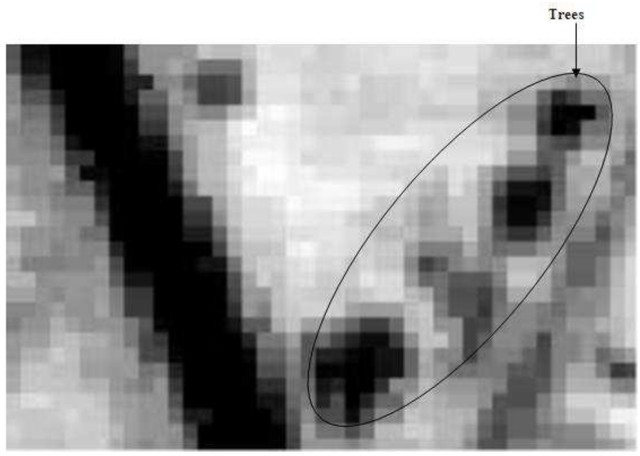

Fig. 4.4. *Trees expression as observed in band 45 from [TIR] region along Western CSR*

Fig. 4.5. *Verification of anomaly in Band 9 [NIR] and band 45 [TIR] through Google Earth*

The above discussion regarding band selection in this research suggests the use of band 9 from the NIR region as the best for identifying prominent land-water boundaries between canals and adjacent land and seepage or water activity sites. This identification, along with band 45 from the TIR region helps identification of false impressions of seepage sites along irrigation canals (as in the example of trees above).

5. Study Area

The total length of the main irrigation canals throughout the Salt River Valley are two hundred miles (321.9 km) (Luckingham, 1989 cited in Yabes et al., 1997). These canals have played a vital role in the development and growth of the Salt River Valley. In Phoenix, AZ, the most positive and interactive relationship between canals and people were seen during 1920-1960 when, in addition to providing water for irrigation purposes, it served as gathering places for farm families (see Southerland, 1989 cited in Yabes et al.,).

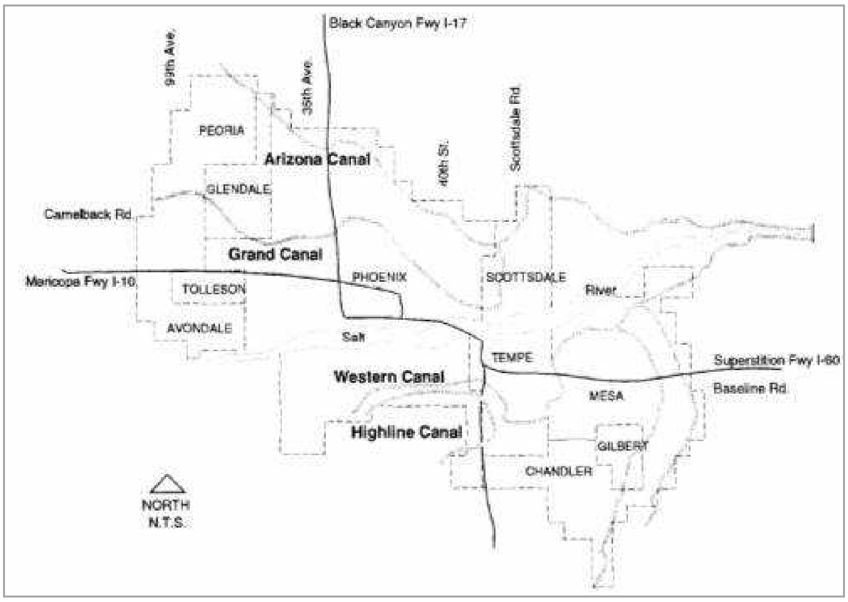

Fig. 5.1. *Location map showing main canals, city boundaries and major roads (Source: Yabes et al., 1997)*

However, these relationships between communities and canals have largely changed due to urbanization of most of the agricultural land in the Phoenix metropolitan area. In this area, there are now more people and fewer farmers than in the early part of the 20th century. In Arizona and other southwestern states semiarid or arid conditions prevail, and the average precipitation across the regions range from 5 to 19 inches annually, with high seasonal, interannual, and long-term variability. During 2002-2004, the southwest experienced some of the most severe drought conditions on record. Tree-ring records of winter precipitation (November-April) show few years as dry as 2002 during the last 1000 years in Arizona (Ni et al., 2002 cited by Sonnett et al., 2006).

The study areas for this research are the canal segments of the Western CSR in metropolitan areas of Phoenix, Arizona. The target area has Upper Left co-ordinates (33.651N, -112.219W) and Lower Right co-ordinates (33.272N, -111.889W). Figure 5.2 is the flight mosaic of the target area.

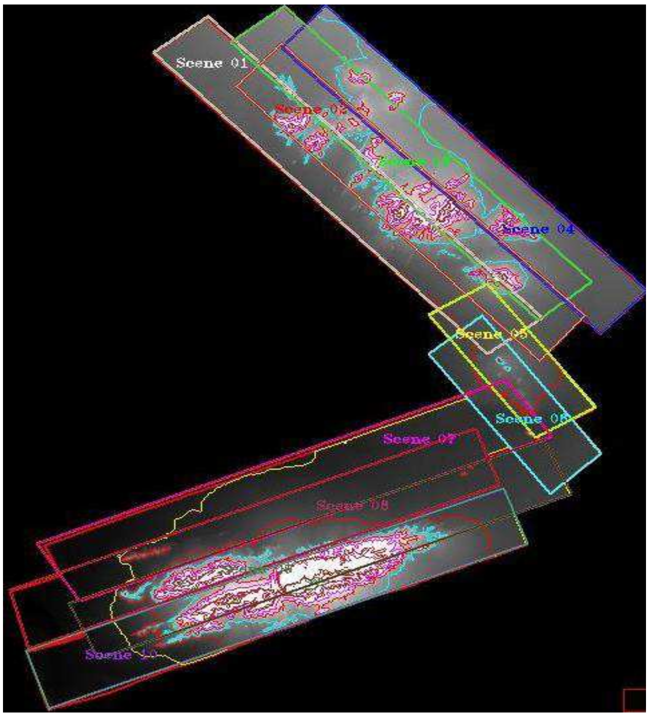

Fig 5.2. *Flight mosaic of 10 MASTER scenes overlaid over DEM data, Phoenix, Arizona*

6. Methods

After studying radiance patterns of MASTER scenes and considering the various parameters as discussed above, it was found that the density slicing technique with band 9 in the NIR and band 45 in the TIR is the best option for the detection of water activity adjacent to the canals. The density slice technique converts the continuous tone of an image into a series of density intervals, each corresponding to a specific range of digital numbers (DN). Different density slices can be shown as separate colors and can be draped over background images (Sabins, 1997 cited in AbdelSalam et. al. (2000). Using Landsat TM band-ratios 5/7 and 3/1, AbdelSalam et al. successfully created clay and Fe alteration index maps by applying the density slicing technique. He also quoted Ramadan et al., as having utilized the density slicing technique for mapping clay- and Fe- rich alteration zones along the Neoproterozoic Allaqi Suture in southern Egypt.

Yamano et al. (2006) used the density slicing technique for delineating the land-water boundary at coral reef coasts (Majuro Atoll, Marshall islands). Klemas et al. (1973) sliced image gray tone variations into increments and then assigned different colors by employing the density slicing technique to delineate the suspended sediment patterns observed from Earth Resources Technology Satellite ERTS-1 over the Delaware Bay during different portions of the tidal cycle. Klemas et al. (1973) demonstrated that color density slicing was a better technique for obtaining reliable results with a modest investment of time and money. Whiteman and Brown (1998) used the density slicing technique to address the problem of grassland conversion to woodland as a result of shrub increase that has caused great concern among rangeland managers around the world (Scifres, 1987, cited in Whiteman and Brown). Whiteman and Brown also used the density slicing technique to segregate shrubs, trees, grass, and soil on the basis of their appearance on the imagery.

6.1. MASTER Data Analysis

In this section, MASTER scenes 1, 2, and 4 (mosaicked and masked) and scene 08 are investigated for seepage, water activity sites, and the possibility of false impressions of seepage sites (such as dense natural vegetation or man-made structures), utilizing the density slicing technique. Different objects on the ground register different ranges of brightness values. But occasionally, similar ranges of brightness values are often registered by different features on the ground. Therefore, gray scales values of band 9 from the NIR region and band 45 from the TIR region were carefully sliced into a series of density intervals in order to give a distinct color to features of interest such as canal water, canal banks, dirt roads, paved roads and vegetation. The following tables show the systematic density slicing of the radiance values in band 9 (0.8690µm) from the NIR region and band 45 (9.744µm) from the TIR region for Scenes 1, 2, and 4 and Scene # 08 in order to single out any anomaly for verification via Google Earth.

6.1.1. Combined Scenes 1, 2, and 4 Mosaicked and Masked

Table 6.1.1. *Gray scale values of selected features in the NIR band*

Type of Band	Band	Wavelength (µm)	Spatial Resolution (m)	Gray scale values	Feature defined in the gray scale range
				180-800	Total gray scale range
NIR	**09**	**0.8690**	**3.9**	180-380	Cyan, Canal water
				380-520	Blue, Canal banks
				520-800	Red, Vegetation, Dirt Rds

6.1.2. Scene 08

Table 6.1.2. *Gray scale values of selected features in the NIR band*

Type of Band	Band	Wavelength (µm)	Spatial Resolution (m)	Gray scale values	Feature defined in the gray scale range
				50-1500	Total gray scale range
				50-450	Cyan, Canal Water
NIR	**09**	**0.8690**	**3.9**	450-700	Blue, water, False impression
				700-850	Orange2,
				980-1500	Red, Dirt Rd, etc.

6.1.3. Combined Scenes 1, 2, and 4 Mosaicked and Masked

Table 6.1.3. *Gray scale values of selected features in the TIR band 45*

Type of Band	Band	Wavelength (µm)	Spatial Resolution (m)	Gray scale values	Feature defined in the gray scale range
				816-1632	Total gray scale range
				816-1020	Cyan, Western CSR & lakes
TIR	**45**	**9.744µm**	**3.9**	1020-1224	Magenta, Grassland, Paved Rds & Parking lots
				1224-1428	Maroon, Bare land, gray rooftops
				1428-1632	Sea green, Building rooftops

6.1.4. Scene 08

Table 6.1.4. *Gray scale values of selected features in the TIR band 45*

Type of Band	Band	Wavelength (µm)	Spatial Resolution (m)	Gray scale values	Feature defined in the gray scale range
				911-1822	Total gray scale range
				911-1139	Cyan, Western CSR & lakes
TIR	**45**	**9.744µm**	**3.9**	1139-1367	Magenta, Dirt Rds & paved Rds
				1367-1594	Maroon, Construction
				1594-1822	Maroon, Rooftops

Figure 6.1.1 shows delineated canal segments in scenes 1, 2, and 3 mosaicked and masked (band-9, [NIR] region) with different ranges of radiance values utilizing density slicing technique.

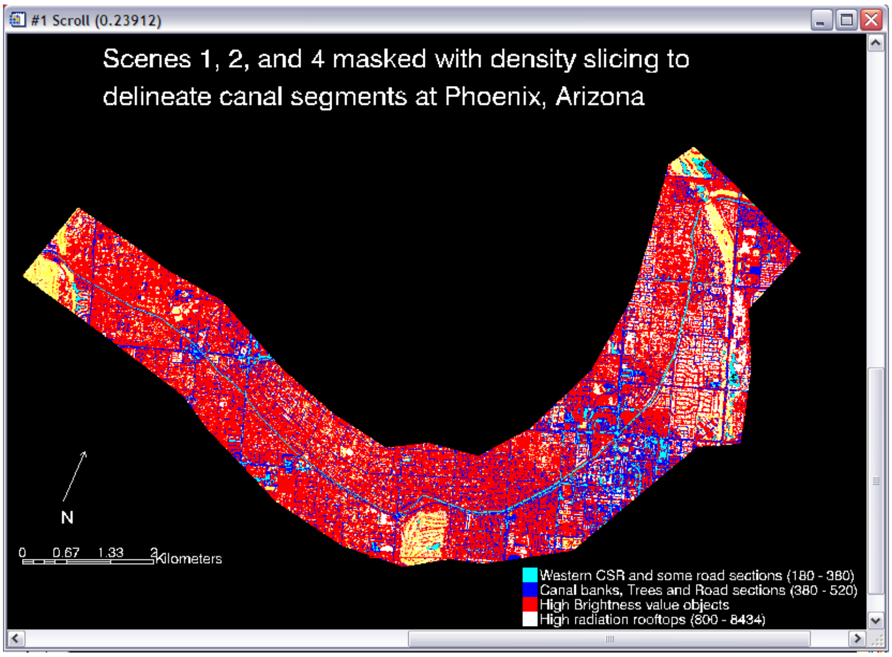

Fig. 6.1.1. *Scenes 1, 2, and 4 masked with density slicing (band-9, NIR region) to delineate canal segments at Phoenix, Arizona*

7. Results and Discussion

7.1. Combined Scenes 1, 2, and 4

In the tables a low range of radiance values (cyan color) in the canal indicate water. Figure 7.1.1 shows that clear water in the western CSR is found to have low radiance values (cyan color) due to the low temperature of water compared to the canal banks (blue color) and dirt roads (red color) along the canal's sides.

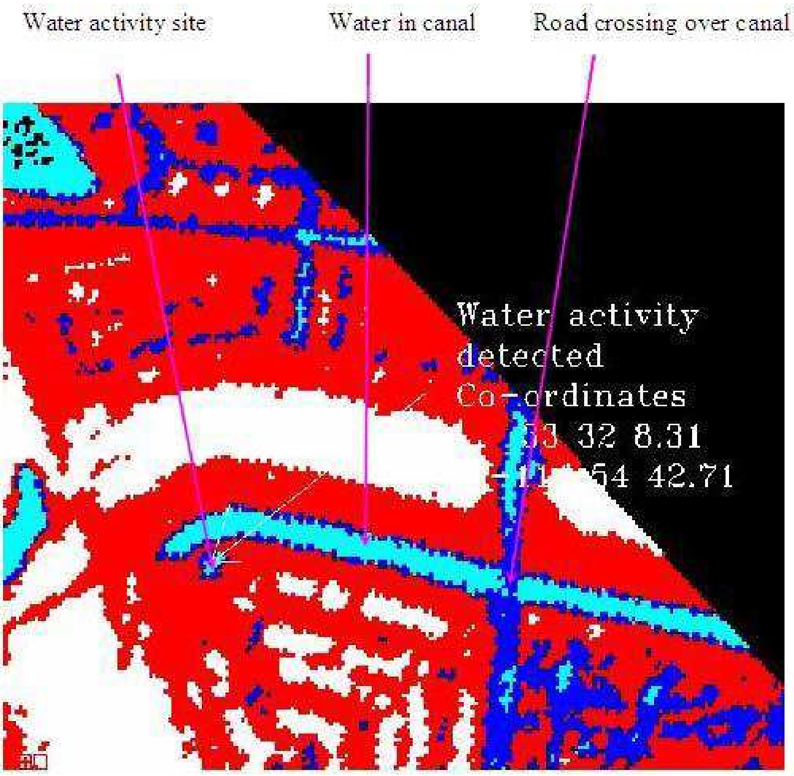

Fig. 7.1.1. *Water in canal is cyan colored representing the lowest radiance values in density slice*

Examination of scene 4 of the combined scenes (1, 2 and 4) revealed a water activity site as shown in figure 7.1.1. A region of interest (ROI) for the above site in the band-9, NIR spectral region (Figure 7.1.2) was processed and the anatomy of the ROI was done by assigning different colors to different increments of radiance values (Figure 7.1.3).

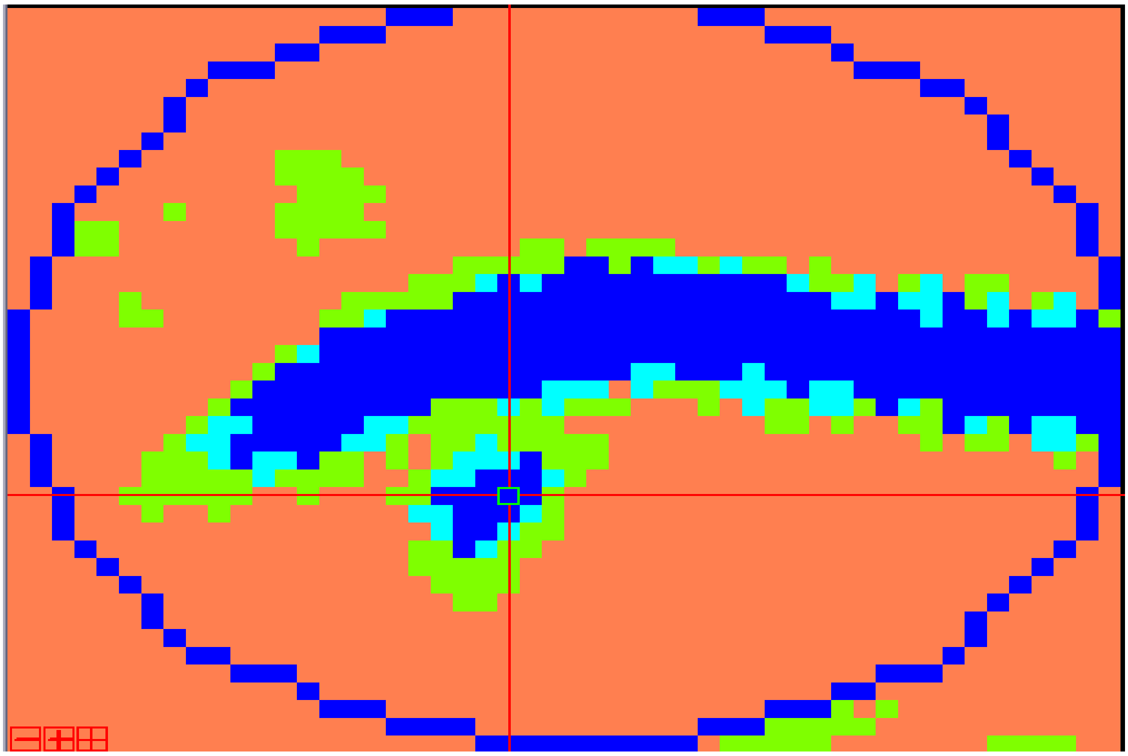

Fig. 7.1.2. *Region of interest for water activity site with application of density slicing*

255	251	254	255	255	222	251	235	233	255	255	255	255	255	255	255	255	255	255	255	255	255	255	255	255	255	255	255	255	255	255	255	255	2
251	222	222	232	197	184	184	233	233	233	255	255	255	255	255	255	255	255	255	255	255	255	255	255	255	255	255	255	255	255	255	255	255	2
219	218	218	213	186	186					255	255	255	255	255	255	255	255	255	255	255	255	255	255	255	255	255	255	255	255	255	255	255	2
215	215	213	211	211	193					255	255	255	255	255	255	255	255	255	255	255	255	255	255	255	255	255	255	255	255	255	255	255	2
215	247	235	211	188	168	168	177	215	215	255	255	255	255	255	255	255	255	255	255	244	255	255	255	255	255	255	255	255	255	255	255	255	2
219	235	235	211	182	182	177	198	198	255	255	255	255	255	255	255	255	212	212	244	255	255	255	230	255	255	255	255	255	255	255	255	255	2
223	240	236	228	228	192	235	254	254	255	255	255	255	255	255	185	179	255	101	101	155	119	230	230	255	226	255	255	255	255	255	255	255	2
223	236	247	255	245	255	255	255	255	255	255	255	196	196	185	179	179	0	0	101	0	47	47	146	53	161	161	255	144	236	255	214	214	2
216	255	255	255	255	255	255	255	224	255	195	97	196	79	0	88	0	0	0	0	0	0	0	0	0	0	0	43	144	144	72	214	140	5
248	255	255	255	255	255	255	178	178	119	97	97	0	0	0	0	0	0	0	0	0	0	0	0	0	0	0	0	0	72	72	21	54	5
255	255	255	255	255	255	122	178	75	0	0	0	0	0	0	0	0	0	0	0	0	0	0	0	0	0	0	0	0	0	21	0	0	5
255	255	255	255	255	255	9	9	0	0	0	0	0	0	0	0	0	0	0	0	0	0	0	0	0	0	0	0	0	0	0	0	0	
255	255	249	255	200	86	9	0	0	0	0	0	0	0	0	0	0	0	0	0	0	0	0	0	0	0	0	0	0	0	0	0	0	
255	229	229	136	28	28	0	0	0	0	0	0	0	0	0	0	0	0	0	0	84	84	30	0	0	43	0	0	0	0	0	0	0	
235	229	136	23	28	0	0	0	0	0	0	0	0	0	0	0	71	71	67	222	84	166	122	122	43	79	79	0	42	42	0	13	13	
235	145	23	23	0	0	0	0	0	0	6	118	115	115	86	174	71	165	171	171	222	243	243	193	235	79	133	191	42	86	158	13	58	1
145	40	40	0	0	0	0	0	68	68	118	183	183	179	183	174	188	222	222	255	255	255	255	255	255	255	191	191	233	158	219	219	130	1
77	40	9	6	0	0	23	33	68	181	214	183	172	88	183	188	159	159	160	255	255	255	255	255	255	255	255	233	255	255	219	255	255	1
122	64	6	52	52	23	108	108	240	181	214	145	88	88	90	1	159	160	188	255	255	255	255	255	255	255	255	255	255	255	255	255	255	2
122	153	138	52	122	200	108	198	255	243	145	43	43	0	0	1	33	117	255	255	255	255	255	255	255	255	255	255	255	255	255	255	255	2
153	186	186	205	252	200	255	255	255	186	120	0	0	0	0	0	117	215	215	255	255	255	255	255	255	255	255	255	255	255	255	255	255	2
235	186	242	255	252	255	255	255	255	244	63	63	0	0	0	73	151	215	255	255	255	255	255	255	255	255	255	255	255	255	255	255	255	2
235	255	255	255	255	255	255	255	255	204	204	38	29	29	53	151	151	238	255	255	255	255	255	255	255	255	255	255	255	255	255	255	255	2
255	255	255	255	255	255	255	255	255	255	180	147	29	93	119	119	238	238	238	255	255	255	255	255	255	255	255	255	255	255	255	255	255	2
255	255	255	254	255	255	255	255	255	244	147	147	158	139	139	209	231	255	255	245	255	255	255	255	255	255	255	255	246	255	255	255	255	2
240	240	254	255	255	255	255	255	255	221	221	158	194	191	182	231	243	243	245	231	231	255	255	255	255	255	255	224	214	255	255	255	255	2
248	246	247	255	255	255	255	255	255	255	255	207	191	191	251	244	243	251	240	231	255	255	255	255	255	255	255	214	214	255	255	255	255	2

Canal water with variation in BV's

Co-ordinates
33 32 8.32 N
(-)111 54 42.72 W

Water standing before diversion gates

Dirt road with canal banks

Fig. 7.1.3. *Brightness values of the region of interest (ROI) to delineate various features on the ground*

To verify this anomaly along the irrigation canal, Google Earth (see: figure 7.1.4) was used to confirm that this is a water activity site.

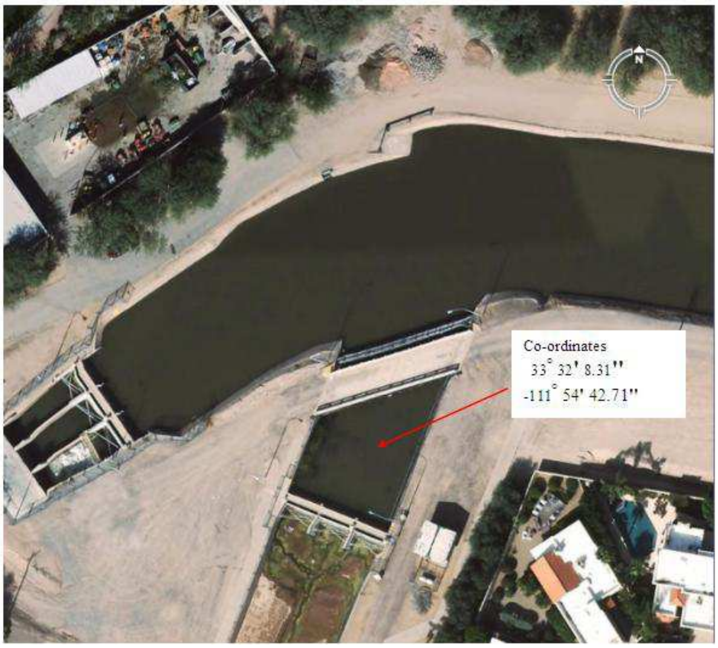

Fig. 7.1.4. *Verification of the water activity site through Google Earth*

More examples of water activity sites and false impressions of activity sites and their verification through Google Earth is provided below to demonstrate that it is straight-forward to discriminate a water activity site from terrain relief, shadows, natural and/or man-made structures etc, using this technique.

7.2. MASTER Scene 08

MASTER Scene 08 is discussed separately because it is the only scene that has agricultural land along the Western CSR. As explained earlier, most of the Phoenix metropolitan areas that were agricultural lands in the past have been converted into urban areas. Analysis of this scene [TIR band-45] shows water activity sites, tree shades and construction along the Western CSR. Figure 7.2.1 shows overall annotation of tree shades, water activity sites and probably a canal breach site.

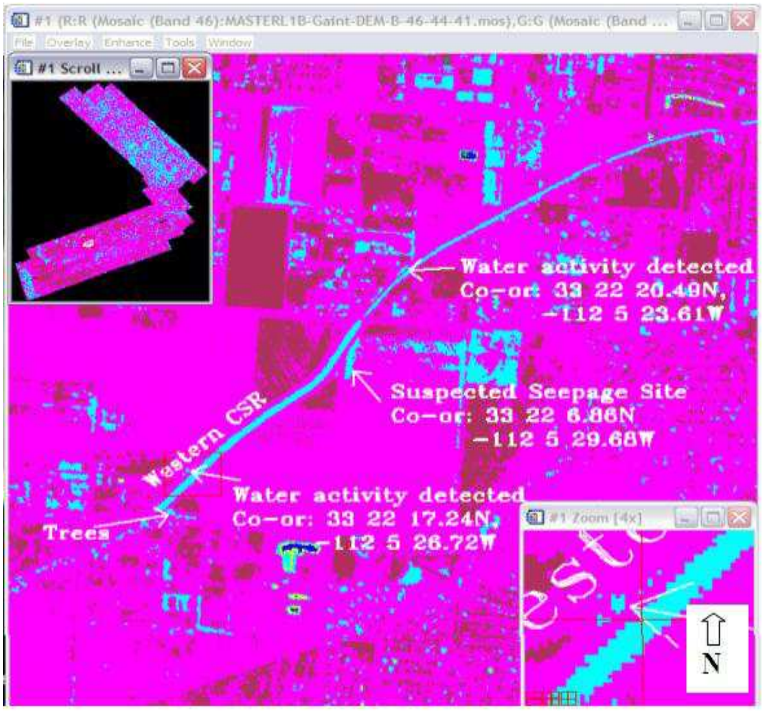

Fig. 7.2.1. *Various anomalies detected [TIR Band 45] in scene 08 are annotated and verified through Google Earth*

One of the anomaly in figure 7.2.1 (Probable location: 33 22 06.88 N, -112 05 29.68 W) is suspected to be canal (seepage or breach) site.

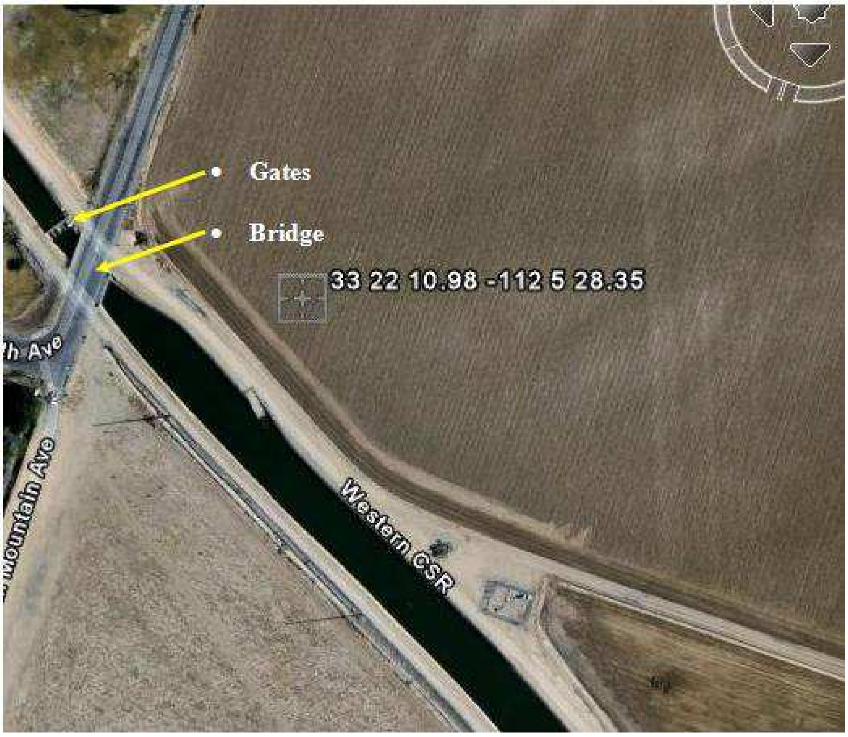

Fig. 7.2.2. *Image of the suspected seepage or canal breach on Google Earth*

Viewing the Google image (Figure 7.2.2) for the anomaly in Figure 7.2.1 reveals that the canal converges before the bridge and is followed immediately by the water regulating gates which control the water flow in canal. The Region of Interest for the same area (Scene 08) was analyzed and assigned different colors to different ranges of the brightness and radiance values (see figures 7.2.3 and 7.2.4).

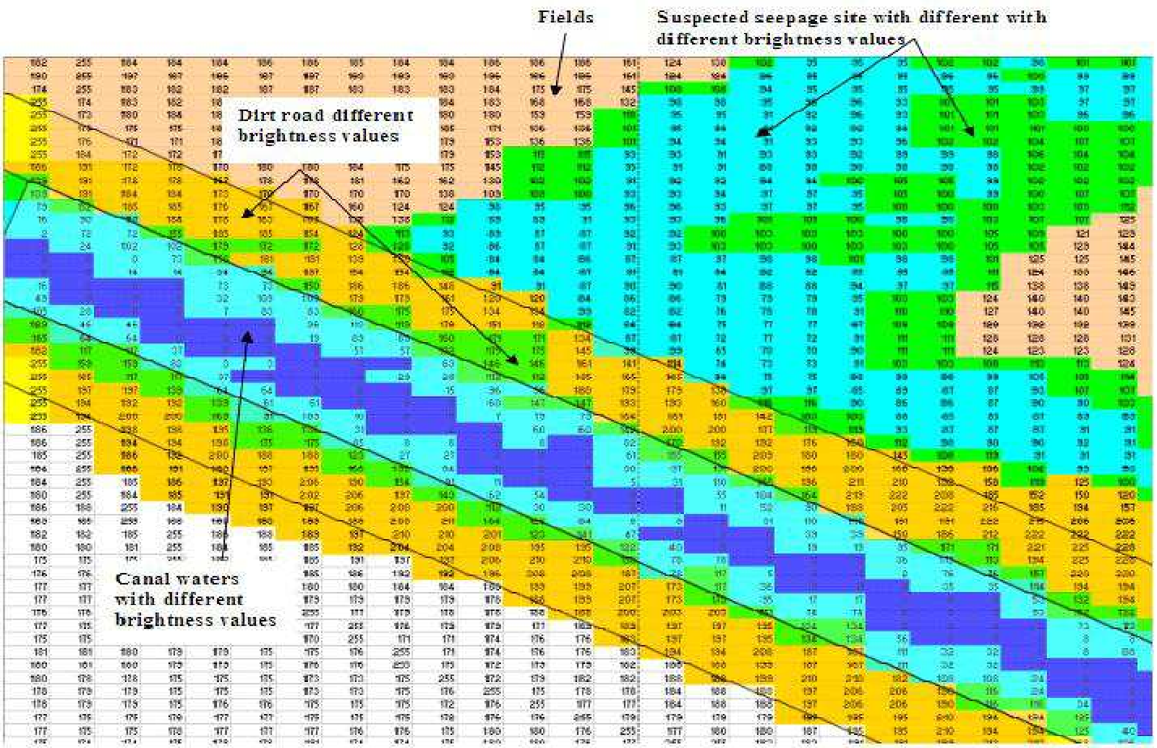

Fig. 7.2.3. *Seepage or canal breach in brightness values (Band-9, [NIR])*

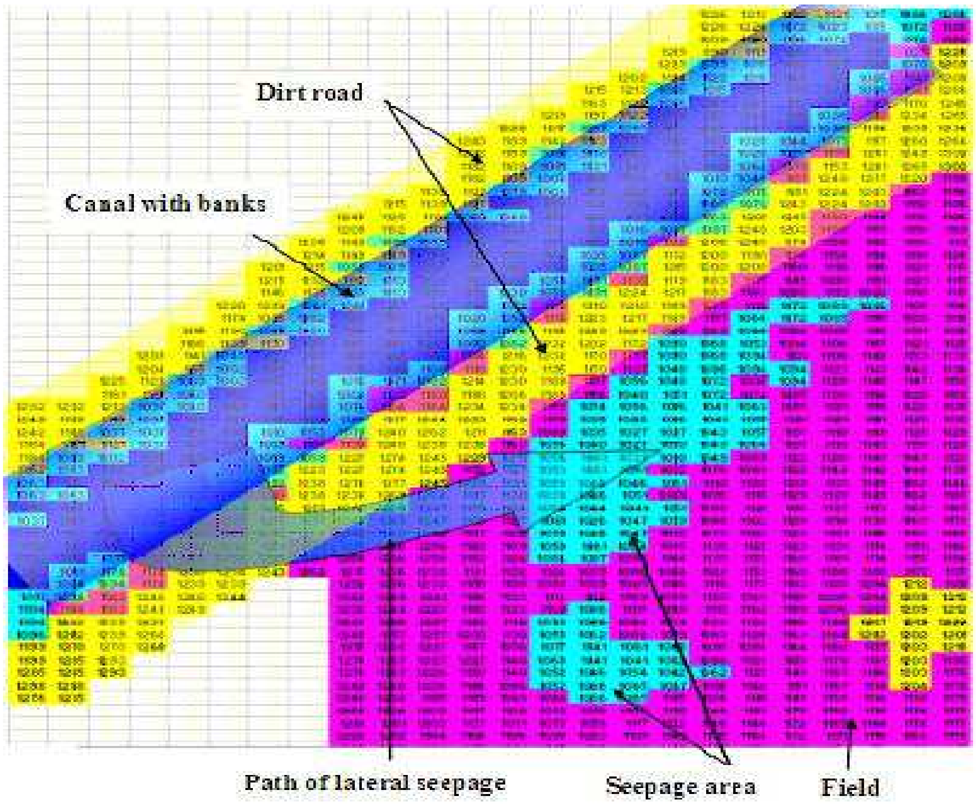

Fig. 7.2.4. *Seepage or canal breach in radiance values (Band-9, [NIR])*

The analysis of the above ROI's in terms of brightness and radiance values allows us to determine that this area was probably breached due to heavy down pouring before the imagery was captured. To confirm this, in figure 7.2.5 a segment of the MASTER scene is overlaid over the DEM data to delineate a micro-watershed surrounding the suspected seepage or canal breach.

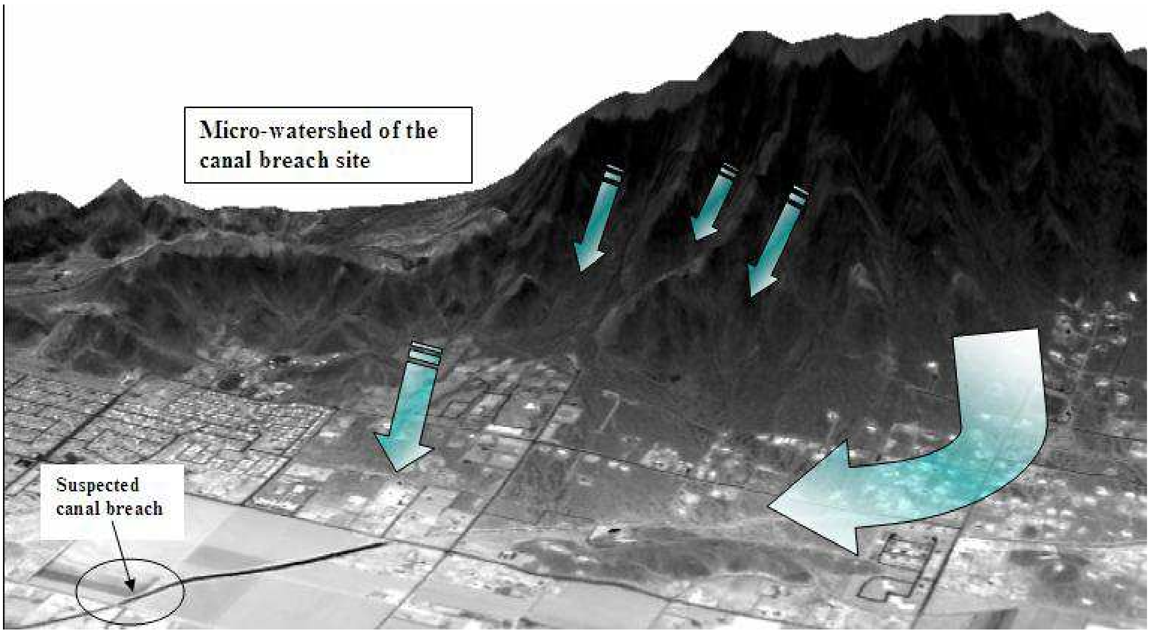

Fig. 7.2.5. *Micro-watershed of the canal seepage or breach site*

The micro-watershed in Figure 7.2.5 reveals that in times of heavy down pouring, due to flooding of the watershed area, the canal was not able to carry more water than its designed capacity and eventually overflowed to the right side of canal downward flow direction. Tree shade produces low radiance values in the TIR bands similar to water radiance values. The reason is that shade, like water, absorbs most of the incident solar flux on it. Tree shade falsely suggests water activity sites (see: Figure 7.26 and 7.27). However, this can also be verified through Google Earth and removed from the list of potential water location sites.

Fig. 7.2.6. *Trees shade gives false identification of water activity site [TIR band-45] is rectified through Google Earth*

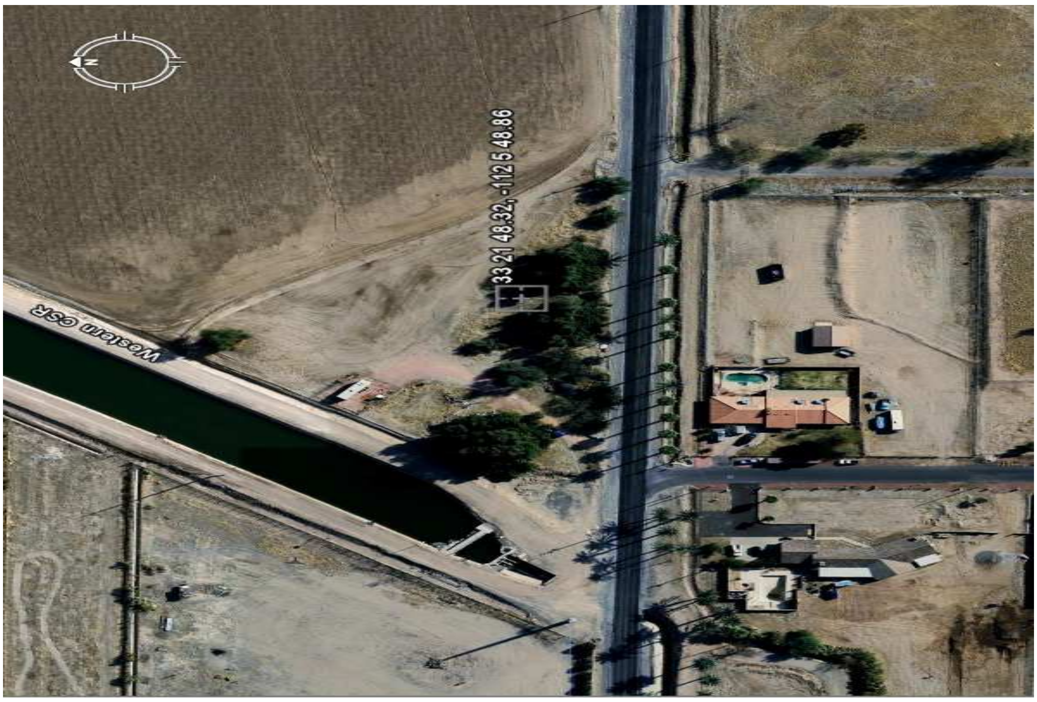

Fig. 7.2.7. *Trees shade giving false identification of water activity site [TIR band-45] is rectified through Google Earth*

8. Conclusions and Recommendations

With the technique proposed in this research, some of the major problems faced by researchers working in this area have been solved. The long-standing problem has been discriminating water activity sites from shade due to trees standing along canal sides, terrain relief, or man-made structures. The accuracy of water activity (wet areas, etc.) detection, or seepage detection, through geospatial techniques reported by various researchers was low. The reason was that these areas created false identification as water activity or seepage sites. The technique we present here can be easily applied, particularly by water resource managers, to monitor the conditions of canals in their jurisdictions. Any anomaly detected using high spatial resolution multispectral imagery can be verified through freely available Google Earth. Canal flow is due to gravity, and in places the flow turns right or left depending upon slope. When augmented by poor soil type, the risk of seepage at turns and on steep slopes is high. Where soil types and curves or steep slopes occur, this technique will allow studying these areas vulnerable to seepage.

As mentioned by Washburn, (2002) canals breach occurs due to natural hazards or man-made activities especially where canals are elevated above the surrounding terrain on one or both sides. At such locations embankment exists, and on occasions leaks develop in the embankment. If left unchecked, these leaks could lead to complete embankment collapses and large areas will come under water, with the loss of valuable water resources in addition to requiring enormous amounts of repair costs. If the water resource managers are properly trained with this technique they can easily investigate any such abnormalities, especially where embankments exists, and can take necessary actions promptly where and when needed. Researchers working in the area of water logging and salinity will also benefit from the use of this research. With this technique, or slight modifications, they can study various processes related to water logging and salinity. Application of this technique to address seepage detection and control will hopefully minimize water logging and salinity problems.

In the near future, it is expected that with technological advancements and drop in cost of acquiring high resolution imagery, computer hardware and software, real time or near real time monitoring of canals for seepage detection besides other investigations will further improve.

Acknowledgements

For this research, Airborne MASTER Datasets of Phoenix, Arizona were made possible with the assistance of Dr. Michael D. King of NASA Goddard Space Flight Center Greenbelt Maryland and Dr. Jeffrey S. Myers of SAIC, Airborne Sensor Facility of NASA Ames Research Center, Moffett Field, California. The ENVI software was provided courtesy of ITT Visual Information Solutions.

References

[1] ABDELSALAM, M. G., ROBERT, J.S., WOLDEGABRAIEL, G. B., 2000, Mapping gossans in arid regions with Landsat TM and SIR-C images: the Beddaho alteration zone in northern Eritrea. Journal of African Earth Sciences 30(4): pp. 903-916.

[2] AHMAD, M. D., 2002, Estimation of net groundwater use in irrigated river basins using geo-information techniques: A case study in Rechna Doab, Pakistan. PhD thesis, Enschede, The Netherlands, Wageningen University.

[3] ASIF, S., AHMAD, M.D., 2002. Using state of the art remote sensing and GIS for monitoring water logging and salinity. Available online at: www.fao.org/docrep (accessed 20 June, 2006).

[4] CHEN, X., WARNER, T.A., CAMPAGNA, D.J., 2007, Integrating visible, near-infrared and short-wave infrared hyperspectral and multispectral thermal imagery for geological mapping at Cuprite, Nevada. Remote Sensing of Environment 110(3): pp. 344 - 356.

[5] DAVID, PIMENTEL., MARIO G., 1994, Food, Land, Population and the U.S. Economy. Available online at: www.dieoff.org/page40.htm (accessed 15 September 2006).

[6] FRAZIER, P.S., and PAGE, K.J., 2000. Water body detection and delineation with Landsat TM data. Photogrammetric Engineering & Remote Sensing 66(12): pp. 1461 - 1467.

[7] GAWAD, S.M.A., IMAM, E.H., Ali, H.M., 1993, This paper is presented at a conference. In 15th International Congress on Irrigation and Drainage, Hague, Netherlands.

[8] KAY JE, GILLESPIE AR, HANSEN GB, PETTIT EC (2003) Spatial relationships between snow contaminant content, grain size, and surface temperature from multispectral images of Mt. Rainier, Washington (USA). Remote Sensing of Environment 86 (2):216-231.

[9] KLEMAS, V., BORCHARDT, J.F., TREASURE, W. M., 1973. Suspended sediments observations from ERTS-1. Remote Sensing of Environment 2: pp. 205 - 221.

[10] METTERNICHT, G.I., and ZINCK, J.A., 2003. Remote sensing of soil salinity: Potentials and constraints. Remote Sensing of Environment 85: pp. 1 - 20.

[11] NELLIS, M. D., 1980. Water management in the North Deschutes unit irrigation district: Geographic perspectives and remote sensing applications. PhD thesis, Oregon State University, US.

[12] NELLIS, M. D., 1982. Application of thermal infrared imagery to canal leakage detection. Remote Sensing of Environment 12(3): pp. 229 - 234.

[13] NELLIS, M. D., 1985. Interpretation of thermal infrared imagery for irrigation water resource management. Journal of Geography 84(1): pp. 11 - 14.

[14] PHIL, K., ZHUPING, S., 2002. New Mexico state, Texas A&M professors do joint study of irrigation canal seepage. Available online at: www.nmsu.edu/~ucomm/Releases (accessed 15 March 2006).

[15] PICKERILL, J. M. MALTHUS, T.J., 1998. Leak detection from rural aqueducts using airborne remote sensing techniques. International Journal of Remote Sensing 19(12): pp. 2427 - 2433.

[16] RUTH, Y., KIM, S., JOHN, S., 1997. Urban waterways: changing historical uses and users in a southwestern desert city. Landscape and Urban Planning 39: pp. 167 - 185.

[17] SAKTHIVADIVEL, R., AMARASINGHE, U.A., Thiruvegadchari, S., 2001, Using remote sensing techniques to evaluate lining efficacy of watercourses. Available online at: www.cgiar.org/iwmi/publs (accessed 05 January 2006).

[18] SNELL, M., 2001. Lining old irrigation canals: Thoughts and trials. Irrigation and Drainage 50(2): pp. 139 - 157.

[19] SONNET, J., BARBARA, .J.M., THOMAS, D.F., GREGG, G., NICHOLAS, R., 2006. Drought and declining reservoirs: Comparing media discourse in Arizona and New Mexico, 2002-2004 Global Environmental Change 16: pp. 95 - 113.

[20] SWAN, C.H., 1978. Middle East - Canals and irrigation problems. The Quarterly Journal of Engineering Geology. 11: pp. 75 - 78.

[21] WACHYAN, E., RUSHTON, K.R., 1987. Water losses from irrigation canals. Journal of Hydrology 92: pp. 275 - 288.

[22] WALKER, S. H., 1999. Causes of high water losses from irrigated rice fields: Field managements and results from analogue and digital models. Agricultural Water Management 40: pp. 123 – 127.

[23] WASHBURN, G. R., 2002. Use of infrared remote sensing for the detection of potential seepage sites along Erie canal. MS thesis, College of environmental science and forestry Syracuse, State university of New York.

[24] WHITEMAN, G. BROWN, R. J., 1998. Assessment of a method for mapping woody plant density in a grassland matrix. Journal of Arid Environments 38: pp. 269 - 282.

[25] YABES R, SHETTER K, SCHNEEMAN J (1997) Urban waterways: changing historical uses and users in a southwestern desert city. Landscape and Urban Planning 39 (2–3):167-185.

[26] YAMANO, H., SHIMAZAKI, H., MATSUNAGS, T., ISHODA, A., MCCLENNEN, C., YOKOKI, H., FUJITA, K., OSAWA, Y., KAYANNE, H., 2006. Evaluation of various satellite sensors for waterline extraction in a coral reef environment: Majuro Atoll, Marshal Islands. Geomorphology 82: pp. 389 - 411.

[27] YOUNG, S. J., JOHNSON, R.B., HACKWELL, J.A., 2002. An in-scene method for atmospheric compensation of thermal hyperspectral data. Journal of Geophysical Research 107(D24): pp. 14-1 - 14-19.